BNL-219910-2020-TECH

EIC-ADD-TN-008

Resistive wall heating in the copper-coated beampipe of the BNL Electron-Ion Collider

S. Verdu-Andres

September 2020

Electron-Ion Collider

Brookhaven National Laboratory

U.S. Department of Energy

USDOE Office of Science (SC), Nuclear Physics (NP) (SC-26)

Notice: This technical note has been authored by employees of Brookhaven Science Associates, LLC under Contract No.DE-SC0012704 with the U.S. Department of Energy. The publisher by accepting the technical note for publication acknowledges that the United States Government retains a non-exclusive, paid-up, irrevocable, world-wide license to publish or reproduce the published form of this technical note, or allow others to do so, for United States Government purposes.

DISCLAIMER

This report was prepared as an account of work sponsored by an agency of the United States Government. Neither the United States Government nor any agency thereof, nor any of their employees, nor any of their contractors, subcontractors, or their employees, makes any warranty, express or implied, or assumes any legal liability or responsibility for the accuracy, completeness, or any third party's use or the results of such use of any information, apparatus, product, or process disclosed, or represents that its use would not infringe privately owned rights. Reference herein to any specific commercial product, process, or service by trade name, trademark, manufacturer, or otherwise, does not necessarily constitute or imply its endorsement, recommendation, or favoring by the United States Government or any agency thereof or its contractors or subcontractors. The views and opinions of authors expressed herein do not necessarily state or reflect those of the United States Government or any agency thereof.

Resistive wall heating in the copper-coated beam pipe of the BNL Electron-Ion Collider*

Silvia Verdú-Andrés†
Brookhaven National Laboratory (BNL), Upton, NY 11973, United States of America
(Dated: September 30, 2020)

Operation in the Relativistic Heavy Ion Collider (RHIC) with higher intensity beams and shorter bunches is limited by the current-induced heat generated in its stainless-steel beam pipes and the existing cryogenic plant capabilities. The hadron beam of the BNL electron-ion collider EIC will use the Yellow ring of RHIC. Its beam pipe, currently a stainless steel tube, could be copper-coated to reduce the dynamic heat load. This paper overviews the derivation of the main expressions used to calculate the dynamic heat load from beam and pipe parameters and presents the heat load per meter expected from the RF surface resistance measurements at cryogenic temperatures of stainless-steel beam pipe samples copper-coated using the Physical Vapor Deposition (PVD) technique for different bunch distributions.

I. INTRODUCTION

The parasitic heating of the beam pipe is one of the several heat sources to consider when designing a new particle accelerator or a facility upgrade that involves higher-intensity beams and/or shorter bunches. The Yellow ring of RHIC will be the storage ring for the BNL electron-ion collider EIC. A large portion of the stainless-steel beam pipe is integrated into the RHIC superconducting magnets operated at 4.6 K. The passage of the EIC's higher intensity beams and shorter bunches through the current Yellow ring beam pipe – a circular cross section tube made of austenitic stainless-steel (SS316LN) – leads to large heat loads that require increased cryogenic plant capacity to prevent a thermal runaway in the superconducting magnets and a possible quench. Copper-coating the RHIC beam pipe could help to decrease its electrical resistivity, thus decreasing the head load to the 4.6 K system. In this framework, a device for in-situ copper-coating of the RHIC beam pipe hass been developed and the cryogenic RF properties of the first samples coated using this device have been evaluated. This Technical Note collects the expressions to calculate the power loss per unit of length for relevant bunch longitudinal-profile distributions. The estimation of the power loss per unit of length computed from experimental data from two copper-coated RHIC beam pipe samples is presented and discussed.

II. RESISTIVE WALL HEATING IN THE ROUND BEAM PIPE OF A CIRCULAR ACCELERATOR

The parasitic heating due to the passage of a single particle bunch through a resistive beam pipe is:

$$P = Q^2 \kappa_{\parallel} \tag{1}$$

where Q is the electric charge of the particle bunch and $\kappa_{\parallel}$ is the loss factor given by:

$$\kappa_{\parallel} = \frac{1}{2\pi}\int_{-\infty}^{+\infty} d\omega\, Z_{\parallel}(\omega)\, h(\omega) = \frac{1}{\pi}\int_{0}^{+\infty} d\omega\, \mathrm{Re}\left\{Z_{\parallel}(\omega)\right\} h(\omega) \tag{2}$$

where $Z_{\parallel}(\omega)$ is the longitudinal impedance of the beam pipe, $h(\omega)$ is the spectral power density of a Gaussian bunch with rms duration σ_t ($h(\omega) = e^{-\omega^2\sigma_t^2}$) and $\mathrm{Re}\left\{Z_{\parallel}(\omega)\right\}$ is the real component of the longitudinal impedance.

A. Longitudinal impedance of a round resistive beam pipe in a circular accelerator

Only the real component of the longitudinal impedance $\mathrm{Re}\left\{Z_{\parallel}(\omega)\right\}$ contributes to the parasitic heating of the beam pipe. For a round beam pipe with radius b in a circular accelerator with perimeter C:

$$\mathrm{Re}\left\{Z_{\parallel}(\omega)\right\} = \frac{C}{2\pi b} R_s(\omega) \tag{3}$$

where R_s is the RF surface resistance of the beam pipe and mainly depends on the material, surface conditions and temperature of the beam pipe. In the case of the normal skin effect:

$$R_s(\omega) = \sqrt{\frac{\omega\mu}{2\sigma_c}} = \frac{1}{\delta\sigma_c} \tag{4}$$

where ω is the angular frequency ($\omega = 2\pi f$) for a given eigenmode with resonant frequency f, μ is the electrical permeability of the cavity volume, σ_c is the electrical conductivity of the cavity walls and δ is the skin depth ($\delta = \sqrt{2/\omega\mu\sigma_c}$). At cryogenic temperatures and for high-frequencies, good electric conductors like copper experience the anomalous skin effect. The expression for the RF surface resistance in the anomalous skin effect theory is [2]:

$$R_s = R_\infty\left(1 + 1.157\alpha^{-0.276}\right), \quad \text{for} \quad \alpha \geq 3 \tag{5}$$

with:

* Work supported by Brookhaven Science Associates LLC under contract no. DE-SC0012704 with the U.S. Department of Energy.
† sverdu@bnl.gov

$$R_\infty = 1.123\times10^{-3}\,\Omega\times\left(\frac{\omega}{2\pi\,\mathrm{GHz}}\right)^{2/3} \tag{6}$$

$$\alpha = \frac{3}{2}\left(\frac{\lambda}{\delta}\right)^2 = \frac{3}{4}\omega\mu\left(\rho\lambda\right)^2\rho^{-3} \tag{7}$$

where ρ is the electrical resistivity ($\rho = 1/\sigma_c$), an intrinsic property of the material quantified by non-time-varying Direct Current (DC) measurements. The ratio between the electrical resistivity at room temperature (300 K) and at the absolute zero (0 K) is the Residual-Resistance Ratio (RRR = ρ_{300K}/ρ_{0K}). The product $\rho\lambda$ is characteristic of a metal; for copper, $\rho\lambda = 6.6\times10^{-16}\,\Omega\,m^2$. Actual losses will be another 20–30% higher than calculated due to surface roughness [3]. Furthermore, when exposed to a magnetic field, the R_s degrades due to the magneto-resistance effect. Fig. 1 shows the degradation of R_s for copper exposed to a magnetic field [4]. The degradation in R_s is larger for higher RRR values. In the EIC, the main degradation of the R_s is expected for the beam pipes inside the arc dipoles, which deliver 3.45 T to steer the 250 GeV protons in its orbit ($\Delta R_s/R_0 = 0.3$ for RRR = 60 copper exposed to 3.45 T).

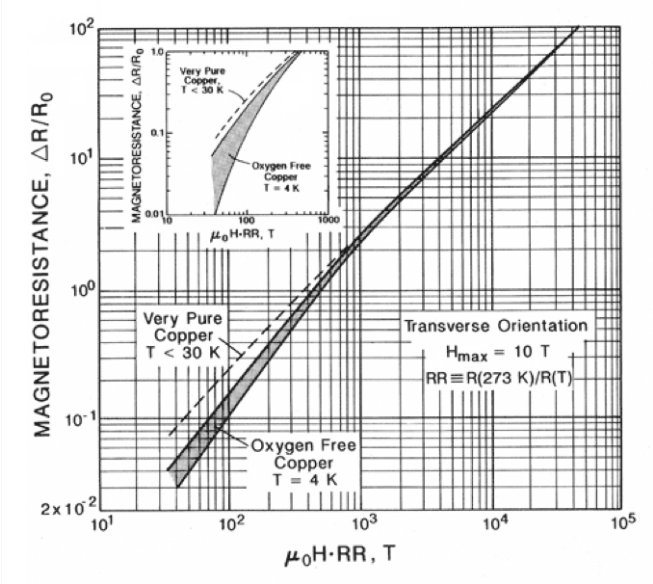

FIG. 1. Degradation of R_s due to magneto-resistance in copper. Plot from Ref. [4].

B. Normalized line density for relevant longitudinal-density bunch profiles

The spectral power density $h(\omega)$ is given by:

$$h(\omega) = \tilde{\lambda}(\omega)\,\tilde{\lambda}^*(\omega) = |\tilde{\lambda}(\omega)|^2 \tag{8}$$

where $\tilde{\lambda}(\omega)$ is the normalized line density of the bunch distribution in frequency domain and $\tilde{\lambda}^*(\omega)$ is its complex conjugate. The normalized line density in frequency domain $\tilde{\lambda}(\omega)$ is calculated from the normalized line density in time domain $\lambda(t)$ and viceversa via a Fourier transform:

$$\tilde{\lambda}(\omega) = \mathscr{F}\{\lambda(t)\} \text{ and } \lambda(t) = \mathscr{F}^{-1}\left\{\tilde{\lambda}(\omega)\right\} \tag{9}$$

where the Fourier transform of a function $f(t)$ with frequency variable ω is here defined as:

$$\mathscr{F}[f(t)](\omega) = \int_{-\infty}^{+\infty} f(t)e^{-i\omega t}dt \tag{10}$$

and the inverse Fourier transform of a function $\tilde{f}(\omega)$ with time variable t is here defined as:

$$\mathscr{F}^{-1}[\tilde{f}(\omega)](t) = \frac{1}{2\pi}\int_{-\infty}^{+\infty} \tilde{f}(\omega)e^{i\omega t}d\omega \tag{11}$$

The distribution selected to describe the bunch profile is relevant when computing the resistive wall heating in the beam pipe caused by the passage of a bunched beam. The Gaussian distribution has long tails (in time-domain), presenting smaller higher frequency components. In first approximation, the longitudinal-density profile of a bunch can be represented by a Gaussian distribution. When the RF bucket is fully filled, a truncated cosine or inverted parabola can better represent the bunch profile. The truncated cosine or the truncated inverted parabola distributions terminate sharply and in consequence present higher frequency components. The normalized line density expressions for some useful distributions are provided in the following.

1. *Gaussian distribution*

For a bunch with Gaussian longitudinal profile in time domain, the normalized line density $\lambda(t)$ is:

$$\lambda(t) = \frac{1}{\sqrt{2\pi}\sigma_t}e^{-\frac{t^2}{2\sigma_t^2}} \quad (\mathtt{t-domain}) \tag{12}$$

The standard deviation of the Gaussian distribution σ_G is equal to the rms bunch length σ_t. In frequency domain:

$$\tilde{\lambda}(\omega) = e^{-\frac{\omega^2\sigma_t^2}{2}} \quad (\mathtt{f-domain}) \tag{13}$$

so the power spectral density becomes:

$$h(\omega) = e^{-\omega^2\sigma_t^2} \tag{14}$$

2. Truncated inverted parabola distribution

In time domain:

$$\lambda(t) = \frac{3}{4\phi^3}\left(\phi^2 - t^2\right) \tag{15}$$

where 2ϕ is the maximum width of the truncated parabola. In frequency domain:

$$\tilde{\lambda}(\omega) = \frac{3}{\phi^3}\left\{\frac{\sin(\omega\phi)}{\omega^3} - \phi\frac{\cos(\omega\phi)}{\omega^2}\right\} \tag{16}$$

The standard deviation for the truncated inverted parabola distribution is:

$$\sigma_P = \phi/\sqrt{5} \tag{17}$$

C. Bunch representation

We imposed common characteristics to the distributions employed in this study:

1. Normalized (same area, same bunch charge): the normalization of the inverted parabola and the Gaussian distributions, respectively, N_P and N_G, are equal to 1.

$$N_P = N_G = 1 \tag{18}$$

2. Same standard deviation:

$$\sigma_G = \sigma_P \tag{19}$$

Fig. 2 shows the line density for different longitudinal-density bunch profiles used in this study following the common characteristics just described.

D. Resistive wall heating in round beam pipe of circular accelerator due to uniformly-filled bunched beam

Assuming a uniformly-filled bunched beam with M bunches, the resistive wall heating or power loss in the beam pipe is:

$$P_M = \frac{Q^2 MC}{2\pi^2 b T_0}\int_0^{+\infty} d\omega\, R_s(\omega)\, h(\omega) \tag{20}$$

where T_0 is the revolution period of a single bunch traveling in a circular orbit of length C ($T_0 = C/(\beta c_0)$) and the factor Q/T_0 is simply the average bunch current I_b. The power loss per unit of length P' is given by the power loss divided by the accelerator perimeter:

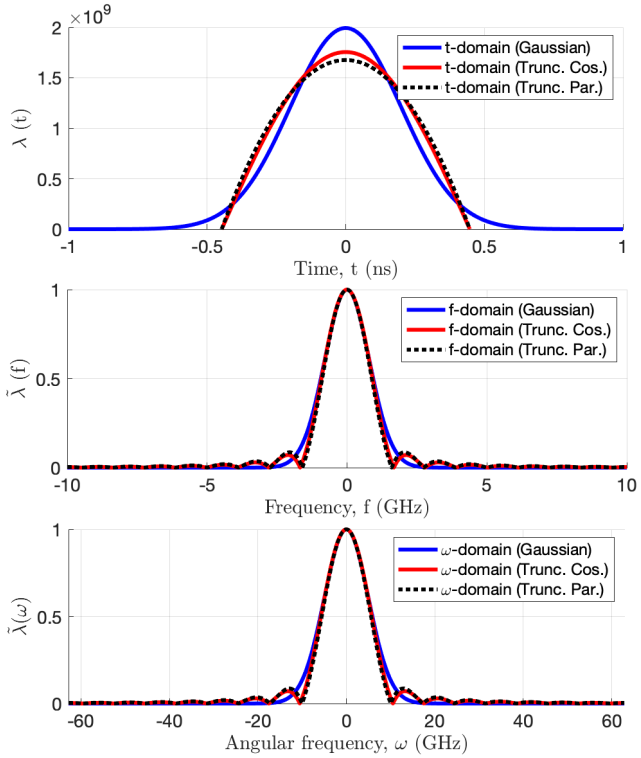

FIG. 2. Normalized line density for relevant longitudinal-profile bunch distributions in time-domain and frequency-domain for 60 mm rms bunch length.

$$P' = \frac{P_M}{C} = \frac{Q^2 M}{2\pi^2 b T_0}\int_0^{+\infty} d\omega\, R_s(\omega)\, h(\omega) \tag{21}$$

The power loss per unit of length for a Gaussian-bunch beam results:

$$P' = \frac{Q^2 M}{2\pi^2 b T_0}\int_0^{+\infty} d\omega\, R_s(\omega)\, e^{-\omega^2\sigma_t^2} \tag{22}$$

Plugging Eq. 4 into Eq. 22 and solving the integral brings us to the following expression:

$$P' = \Gamma\left(\frac{3}{4}\right)\frac{Q^2 M}{4\pi^2 b T_0}\sqrt{\frac{\mu}{2\sigma_c}}\left(\frac{1}{\sigma_t}\right)^{\frac{3}{2}} \tag{23}$$

III. MOTIVATION

Operation with the highest luminosity proton beam is expected to generate a power loss per unit of length of about 0.75 W/m in the stainless-steel beam pipes of the RHIC SC magnets. This value is calculated from Eq. 23 for Gaussian bunches using the physical properties of the RHIC beam

pipe summarized in Table I. The proton beam parameters for the high luminosity scenario are listed in Table II. Such high heat load to the 4.6 K system is undesired because it requires higher cryogenic plant capacity to prevent thermal runaways and possible quenches. Coating the beam pipe with a thin layer (5-10 µm) of copper could reduce the dynamic heat load below 0.5 W/m thanks to the higher electrical conductivity of copper at cryogenic temperatures.

TABLE I. Physical properties of the RHIC beam pipe

Beam pipe radius	b	3.46×10^{-2}	m
Electric conductivity (SS316LN, 4.6 K) [8]	σ_c	1.69×10^{6}	S/m

TABLE II. Beam parameters for the highest luminosity scenario of the EIC [7]

Scenario		Highest Lumi	
Proton beam energy	E	275	GeV
Bunch number	M	1160	–
RMS bunch length	σ_z	6×10^{-2}	m
Charge per bunch	Q	6.881×10^{10}	ppb
Bunch revolution period	T_0	12.8×10^{-6}	s

A. Herscovitsch developed a mole for in-situ copper-coating of the stainless-steel beam pipes inside the RHIC arc dipoles [9]. A test campaign followed to evaluate the RF surface resistance in sample tubes coated with this device and estimate the losses in the beam pipe.

IV. MATERIALS & METHODS

Two sample tubes were copper-coated by PVI Inc. (California, USA) using the in-situ mole. The coating was performed following the Physical Vapor Deposition (PVD) technique [10]. One sample tube was coated with a 10 µm copper layer (PVI-00-10) while another received a 5 µm copper layer (PVI-00-05). The thickness of the applied layers should suffice when copper has a large RRR. Visual inspection of the two samples did not raise concerns about possible adhesion issues.

Each sample tube was tested individually at cryogenic temperatures using the folded coaxial resonator expressly designed for this purpose by J. M. Brennan [11]. The folded coaxial resonator, shown in Fig. 3, allows measuring the RF surface resistance of the sample tube for several resonant modes in a broad frequency band from 180 MHz (fundamental mode) to 4 GHz. The proton bunches of EIC are about 5 cm long, so this range covers sufficiently the frequency range of interest (see bunch profile in Fig. 2). The description of the in-situ mole and the folded coaxial resonator is out of the scope of this paper. The RF surface resistance of each sample tube was calculated for each mode via:

$$R_s(\omega_i) = G(\omega_i)/Q_l(\omega_i) \tag{24}$$

using the loaded Q (Q_l) measured with the network analyzer for each resonant mode up to 4 GHz and the geometry factor G for each eigenmode ω_i retrieved from CST Microwave Studio simulations. Table III lists the $G(\omega_i)$ for all the relevant modes. The folded coaxial resonator is operated at 4.6 K, when the Q_l is dominated by the losses in the sample tube (the antennae are set to be weakly coupled; the inner coaxial tubes are made of niobium, which becomes superconductor below 9.2 K; the spring seals are plated with SnPb, another material that becomes superconductor circa 7.5 K [12]). When possible, the antennae are positioned for critical coupling to have an additional measurement of Q_l.

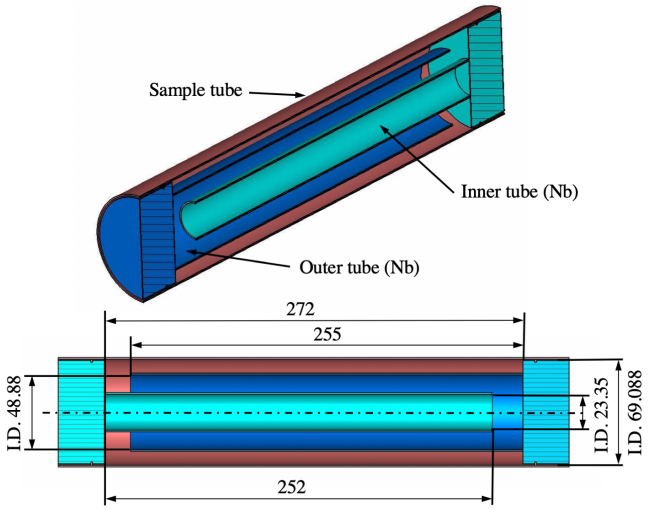

FIG. 3. The folded coaxial resonator: [top] cross section of perspective view identifying the main parts and materials, and [bottom] cross section of side view with main dimensions in mm.

TABLE III. Geometric factor for each eigenmode of the folded coaxial resonator employed to evaluate the RF surface resistance of the tube samples

Frequency f (MHz)	Geometry factor G (Ω)	Frequency f (MHz)	Geometry factor G (Ω)
180	18	2121	239
399	66	2515	567
762	112	2690	285
976	131	3098	821
1345	231	3258	321
1550	188	3677	1255
1930	376	3822	348

To compare the properties of bulk and coated copper and understand possible limitations of the test device and measurement technique, a copper sleeve was made out of a

0.508 mm-thick copper sheet and tested in the folded coaxial resonator at 4.6 K. The thickness is about two orders of magnitude larger than the skin depth of the lowest mode in the folded coated resonator for copper at room temperature.

V. MEASUREMENTS

Figure 4 shows the Q_0 measured for resonant modes of the folded coaxial resonator in the range between 180 MHz and 4 GHz. Three data sets are displayed: 1) copper sleeve; 2) PVI-00-10 tube sample and 3) PVI-00-05 tube sample. In addition, the plot includes the expected Q_0 for RRR = 5 copper at 4.6 K in the anomalous skin effect theory for the reader's reference. Some observations and comments:

- Looking at the expected values, starting from mode at 1550 MHz, the Q_0 goes up and down for every other mode. This is a consequence of the geometry factor (see Table III). Over the whole range, Q_0 increases with frequency.
- While the copper sleeve shows greater Q_0 than for RRR = 5 copper at low frequencies, it drops from mode 1345 MHz upwards. The reason was identified and resolved for the sample tube measurements. Crosstalk between the two antennae introduced a broad peak which frequency depended on the penetration of the antennae. The copper sleeve will be retested.
- Similar losses for PVI-00-10 and PVI-00-05 despite different thickness.

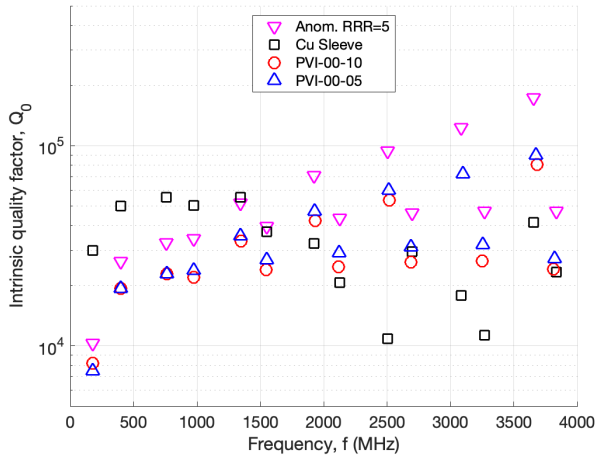

FIG. 4. Measured Q_0 at 4.6 K for different resonant modes in the folded coaxial resonator loaded with: copper sleeve; PVI-00-10 sample tube, and PVI-00-05 sample tube. Expected Q_0 for RRR = 5 copper at 4.6 K in the anomalous skin effect theory.

VI. RESULTS & DISCUSSION

Figure 5 shows the R_s calculated from the measured Q_0 of tube samples and copper sleeve. In addition, it displays the expected R_s for different RRR values in the normal skin effect theory and the anomalous skin effect theory. Two data points from Ref. [2] (green diamonds) are included to compare our results with other coating attempts of copper on stainless-steel tubes. Some observations and comments:

- "Fit" to data leads to RRR = 2.7 (magenta curve).
- Up to 2.7 GHz, barely no difference between PVI-00-05 (blue data set) and PVI-00-10 (red data set) despite different coating thickness.
- The R_0 calculated from the PVI-00-10 sample tube data for frequencies above 2.7 GHz shows an unexpected trend. We suspect that the crosstalk mode had not been correctly suppressed at the time this sample was evaluated. For the PVI-00-05 sample test, a hole was re-machined to better accommodate the bushing that shields one antenna from the other.

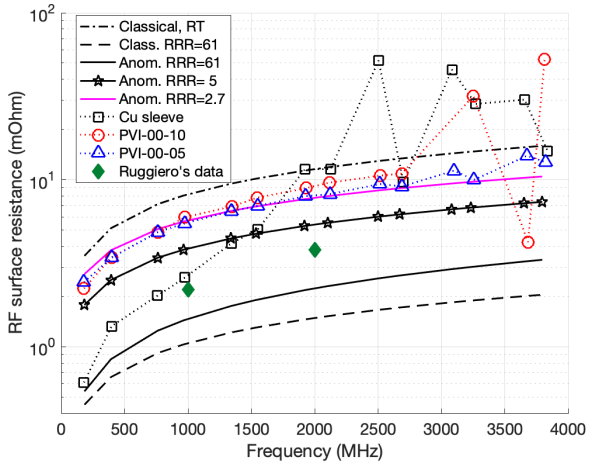

FIG. 5. Calculated R_s for different resonant modes in the folded coaxial resonator loaded with: a) PVI-00-10 sample tube, b) PVI-00-05 sample tube.

The measured R_s for the two sample tubes is used to evaluate the expected heat load in the coated RHIC beam pipe given the current coating quality achieved. To compute the expected power loss per unit of length in the EIC beam pipe, the R_s calculated from experimental data at discrete frequencies is fitted by a spline. The resulting fit is plugged into Eq. 21. The integral is truncated at 2.7 GHz for computation using data from the PVI-00-10 sample and at 3.8 GHz from the PVI-00-05 sample. Fig. 6 shows the power loss per unit of length and frequency computed from the PVI-00-10 sample data. Fig. 7 has the same content but evaluated from the PVI-00-05 sample data. The calculation is performed for the beam spectrum of a uniformly-filled train of bunches with Gaussian and truncated inverted parabola distributions.

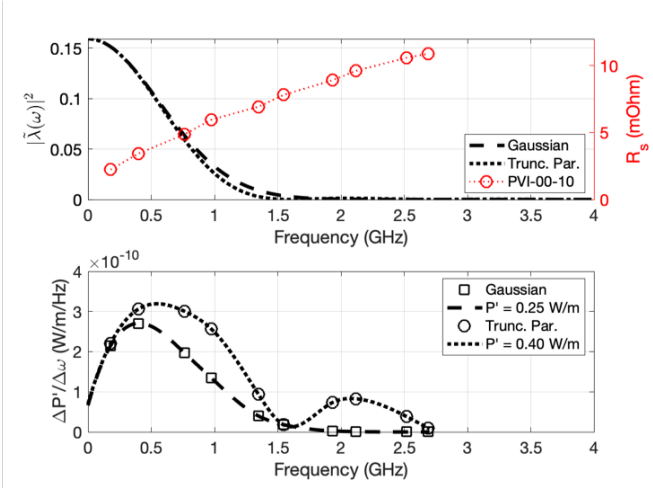

FIG. 6. [Top] Power spectrum density for the highest intensity EIC beam (in black) shown together with RF surface resistance calculated from experimental data taken for PVI-00-10 tube sample (in blue). [Bottom] Power loss per unit of length and frequency over the frequency range of interest. Two bunch distributions considered: Gaussian (dashed line); truncated inverted parabola (dotted line).

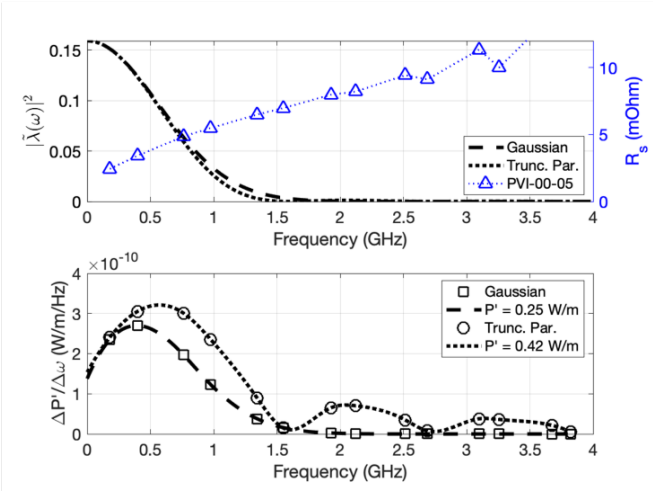

FIG. 7. [Top] Power spectrum density for the highest intensity EIC beam (in black) shown together with RF surface resistance calculated from experimental data taken for PVI-00-05 tube sample (in blue). [Bottom] Power loss per unit of length and frequency over the frequency range of interest. Two bunch distributions considered: Gaussian (dashed line); truncated inverted parabola (dotted line).

The power loss per unit of length is strongly dependent on the bunch distribution. It amounts to 0.25 W/m for the Gaussian bunches, and about 0.40 – 0.42 W/m for the truncated bunches. These values solely consider the R_s measured for the samples, which includes for example the influence of surface roughness on the R_s. The computed values do not include the effects of the large magnetic field in the RHIC arc dipoles. For low RRR, the magneto-resistance effect degrades R_s about 2%, thus increasing the power loss by the same factor. A safety margin of 20% is added to compute the final power loss. Table IV summarizes the power loss calculated for each scenario.

TABLE IV. Total power loss evaluated from PVI-00-05 sample data including magneto-resistance effect and safety margin

Bunch distribution	Gaussian	Truncated	
Power loss evaluated from data	0.25	0.42	W
Magneto-resistance effect (2%)	0.05	0.08	W
Safety margin (20%)	0.06	0.10	W
Total power loss	0.36	0.60	W

Frequencies above 2.7 GHz have some non-negligible contribution (about 5% of the total power loss) for truncated bunches. A better understanding of the longitudinal particle distribution in the EIC bunches would help to evaluate with more accuracy the expected power loss. For example, other hadron machines have bunches which are better described by qGaussian [13] and binomial [14] distributions.

VII. CONCLUSIONS AND OVERVIEW

The total power loss is close to the current goal of 0.5 W/m. While this goal is being reviewed, new samples are being prepared using the Ion Assisted Deposition (IAD) technique, which should provide higher RRR copper films. Multi-physics simulations will study the heat extraction through the cooling channels of the RHIC arc dipoles and the temperature distribution in the cross section of these magnets during coating and operation. These studies will enable us to define a more accurate goal for the power loss in the beam pipes. Another study will focus in analyzing the possible effects of a sudden magnet quench on the copper film.

We are confident that crosstalk between antennae is sufficiently mitigated. A series of tests are planned to fully validate the test device and measurement technique of the coated samples. A first cryogenic RF test will use a partially SnPb-plated copper sleeve. The extension of surface plated is sufficient to bring the Q_0 up to 10^6. With this test, we will get the maximum measurable Q_0 and the contribution of joints and antennae to the global Q_0. A second cryogenic RF test will measure again the copper sleeve. Repeating this test is important to find the maximum Q_0 reachable by bulk copper. We will measure Q_0 at different temperatures (ratio between room temperature and 4K provides RRR). Coupling of the probes may need to get adjusted from mode to mode. With cooldown, frequency will change due to: 1) thermal contraction and 2) R_s variation with T leading to different skin depth [15]. We also intend to continue performing DC measurements at room temperature and plan to setup a bench for DC measurements at cryogenic temperatures to determine the RRR of samples and copper sleeve. Thick layers may suffer more adhesion issues with thermal

cycling than thin layers. For this reason, we plan to perform thermal cycling and pull tests also on thicker layer samples to evaluate their adhesion.

N.B. By the time I am wrapping up this technical note, the beam screen has been adopted as baseline to mitigate the beam-induced losses in the EIC hadron ring and further understanding of the heat load threshold has been reached. In addition, the highest resistive-wall heating comes from the highest luminosity scenario, not from the highest center-of-mass scenario used across this note.

ACKNOWLEDGEMENTS

The author would like to thank Michael Blaskiewicz, Joe Tuozzolo, Roberto Than and Binping Xiao (BNL) for useful discussions and Ady Herscovitch (BNL) and PVI Inc. for providing the samples. Thanks also to Paul Orfin, Ken Riker, Dave Nace II from the C-AD Cryogenic Group of BNL and to Dick Spitz from the C-AD RF Group of BNL for support in conducting the measurements. Special thanks are for Joseph Michael Brennan who led the cryogenic RF measurements.

[1] Electromagnetic and Nuclear Interactions, in “Handbook of Accelerator Physics and Enginneering", A. W. Chao, K. H. Mess, M. Tigner and F. Zimmermann, Ed., 2nd edition, World Scientific, Singapore (2013).

[2] W. Chou and F. Ruggiero, “Anomalous skin effect and resistive wall heating”, LHC Project Note 2 (SL/AP), CERN, Geneva (Switzerland, 1995): http://cds.cern.ch/record/691905/files/project-note-2.pdf

[3] A. Hernández, E. Martín, J. Margineda and J. M. Zamarro, “Resonant cavities for measuring the surface resistance of metals at X-band frequencies", J. Phys. E: Sci. Instrum. **19** (1986).

[4] https://www.copper.org/

[5] Relativisitc Heavy Ion Collider Configuration Manual (2006): https://www.bnl.gov/cad/accelerator/docs/pdf/RHICConfManual.pdf

[6] M. Blaskiewicz, “Copper coating specification for the RHIC arcs”, BNL Note C-A/AP/#413, Upton, NY (USA, 2010).

[7] V. Ptitsyn, “eRHIC parameter v.6.0.”, priv. communication (email, 31 May 2019).

[8] National Bureau of Standards Special Publication 260 - 46, “Thermal conductivity and electrical esistivity standard reference materials: austenitic stainless steel, SRM’s 735 and 798, from 4 to 1200 K".

[9] A. Hershcovitch et al., “Novel techniques and devices for in-situ film coatings of long, small diameter tubes or elliptical and other surface contours", Journal of Vacuum Science & Technology B 33, 052601 (2015); https://doi.org/10.1116/1.4927373.

[10] A. Hershcovitch et al., “Novel technique ion assisted in-situ coating of long, small diameter, accelerator beam pipes with compacted thick crystalline copper film", in Proc. IPAC’19. https://ipac2019.vrws.de/papers/thpts080.pdf

[11] J. M. Brennan, priv. comm. (2017).

[12] A. Nie and M. Williams, “Determination of the critical field and critical temperature for various Type I and Type II metals and alloys" (2016): http://users.physics.harvard.edu/~mwilliams/documents/superconductivity.pdf

[13] J. F. Esteban Mueller (Ph.D. thesis): https://cds.cern.ch/record/2196930/files/CERN-THESIS-2016-066.pdf

[14] A. Lasheen (Ph.D. thesis): https://cds.cern.ch/record/2270190/files/CERN-THESIS-2017-068.pdf

[15] Topic discussed by different authors, for example: J. D. Jackson, “Classical Electrodynamics", 3rd edition, John Wiley & Sons Inc. (1999), page 373; D. M. Pozar, “Microwave Enginneering", 3rd edition, John Wiley & Sons Inc. (2005), page 268.